Ubiquitous and Kidney-Specific Subunits of Vacuolar H^+-ATPase Are Differentially Expressed during Nephrogenesis

François Jouret,* Céline Auzanneau,† Huguette Debaix,* Ge-Hong Sun Wada,‡ Chrystel Pretto,† Etienne Marbaix,† Fiona E. Karet,§ Pierre J. Courtoy,† and Olivier Devuyst*

**Division of Nephrology and †ICP Cell Unit, Université catholique de Louvain, Brussels, Belgium; ‡Doshisha University, Kyoto, Japan; and §Department of Medical Genetics, Cambridge University, Cambridge, United Kingdom*

The vacuolar H^+-ATPase (V-ATPase) is a ubiquitous multisubunit pump that is responsible for acidification of intracellular organelles. In the kidney, a particular form of V-ATPase, made of specific subunits isoforms, has been located at the plasma membrane of intercalated cells (IC). Mutations in genes encoding IC-specific subunits cause infant distal renal tubular acidosis (dRTA), suggesting that the segmental distribution of these subunits is acquired at birth or during early infancy. However, the comparative ontogeny of the IC-specific *versus* the ubiquitous subunits of V-ATPase and the mechanisms involved in their segmental expression remain unknown. Real-time reverse transcription–PCR, *in situ* hybridization, immunoblotting, immunostaining, and subcellular fractionation analyses characterized the expression and distribution of V-ATPase subunits, transcription factors, and differentiation markers during mouse nephrogenesis. Ubiquitous A, E1, B2, G1, and C1 subunits showed an early (embryonic day 13.5 [E13.5]) and stable expression throughout nephrogenesis, followed by a slight increase around birth. The developmental pattern of a1 was bimodal, with early induction, gradual decrease during organogenesis, and neonatal increase. These patterns contrasted with the later (from E15.5) and progressive expression of IC-specific a4, B1, G3, and C2 subunits, after the induction of the forkhead transcription factor Foxi1. From E15.5, Foxi1 mRNA was detected in IC, where it co-distributed with B1 in late nephrogenesis. Immunostaining showed that the distribution of ubiquitous E1 and B2 was acquired from E15.5, whereas a4 was located in IC during late nephrogenesis. Subcellular fractionation showed that in both fetal and mature (cortex and medulla) kidneys, E1 and a4 were located in endosomes. These data demonstrate a differential expression and a coordinate regulation of IC-specific *versus* ubiquitous V-ATPase subunits during nephrogenesis. They provide new insights into the complex regulation of V-ATPase subunits, the maturation of IC along the nephron, and the pathophysiology of hereditary dRTA.

J Am Soc Nephrol 16: 3235–3246, 2005. doi: 10.1681/ASN.2004110935

The vacuolar-type proton ATPase (V-ATPase) is a ubiquitous multisubunit pump that is essential for the acidification of intracellular organelles by coupling ATP hydrolysis to transmembrane proton transport (1). The V-ATPase has been located in a variety of intracellular compartments, including clathrin-coated vesicles, endosomes, and lysosomes. Acidification of these intracellular organelles is a prerequisite for a number of important intracellular processes, such as ligand-receptor dissociation, receptor recycling and ligand degradation, storage, or intracellular targeting (2). In addition to its intracellular distribution, V-ATPase has been located in the plasma membrane of specialized epithelial cells of the kidney and epididymis, as well as in the ruffled border membrane of osteoclasts, where it functions in urinary or semen acidification and in bone resorption, respectively (3).

The structure of V-ATPase includes at least 13 different subunits that form two functional domains, V0 and V1 (Figure 1) (3,4). According to quantitative amino acid analysis, the transmembrane V0 domain contains five different subunits that are organized into a complex that is responsible for proton translocation. The cytosolic V1 domain, which involves eight subunits, catalyzes ATP hydrolysis and provides the energy necessary for active proton transport. When located to the plasma membrane, the overall structure of V-ATPase is very similar, but specific isoforms of V0 and V1 subunits are present (5).

The subunit isoforms of the V-ATPase are encoded by distinct genes, with tissue-specific expression patterns. In the kidney, the V-ATPase is essentially distributed in two cell types that are involved in acid–base homeostasis: the proximal tubule cells (PTC) and the intercalated cells (IC) of the collecting duct (CD) (5,6). In PTC, the V-ATPase has been located on the apical side, where it participates in HCO_3^- reabsorption (7). In addition, V-ATPase is responsible for correct vesicular acidification along

Received November 12, 2004. Accepted July 26, 2005.

Published online ahead of print. Publication date available at www.jasn.org.

Address correspondence to: Dr. Olivier Devuyst, Division of Nephrology, Université catholique de Louvain, 10 Avenue Hippocrate, Brussels, Belgium B-1200. Phone: +32-2-764-1855; Fax: +32-2-764-5455; E-mail: devuyst@nefr.ucl.ac.be

ISSN: 1046-6673/1611-3235

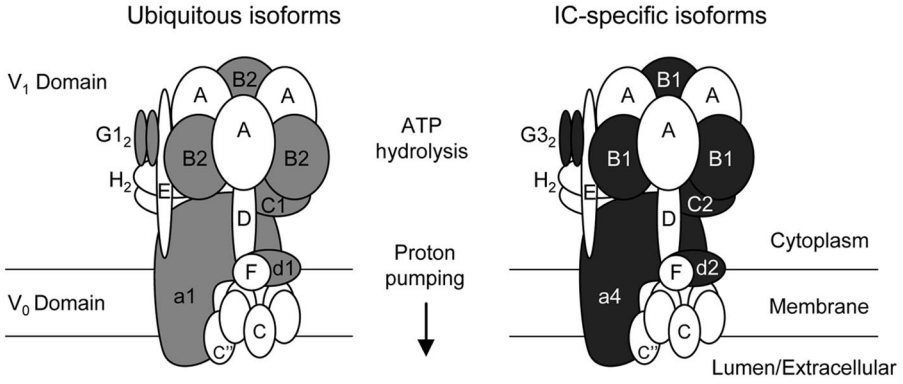

Figure 1. Structural model of the vacuolar type H^+-ATPase (V-ATPase). The transmembrane V0 domain of the mammalian V-ATPase is organized into a complex of $a(c)_{4\text{ to }5}\,c''d$, whereas the cytosolic V1 domain has a stoichiometry of $A_3B_3CDEFG_2H_2$. The ubiquitous and the intercalated cell (IC)-specific alternate isoforms of V0 and V1 subunits are colored. In the plasma membrane of murine IC, a4, d2, B1, C2, and G3 substitute ubiquitous a1, d1, B2, C1, and G1, respectively. This model was modified from the yeast model to represent the mammalian V-ATPase complex (adapted with permission from reference 5). Note that the presence of up to three copies of each E and G per V-ATPase complex has been suggested from analysis of Coomassie staining (4) and that the existence of the c′ subunit in mammals is uncertain (42).

the endocytic pathway, which is essential for receptor-mediated endocytosis and proper intracellular membrane targeting (8). In IC, a specialized form of V-ATPase, made of tissue-specific V0 and V1 subunits isoforms, mediates transepithelial proton transport, ensuring correct urinary acidification (7).

Despite the pivotal role of V-ATPase in acid–base homeostasis, the ontogeny of its subunits in the nephron remains unknown. During pre- and postnatal nephrogenesis, the expression and maturation of several transporters implicated in acid–base homeostasis is tightly regulated to compensate the acid-generating process of growth (9,10). Term neonates are indeed characterized by lower values of blood pH than adults, reflecting an incomplete kidney maturation to reabsorb HCO_3^- (11). The targeted disruption of the V0 c subunit in mouse leads to early fetal lethality by lack of postimplantation development (12). By contrast, mutations in *ATP6V0A4* and *ATP6V1B1* genes, encoding IC-specific V0 a4 and V1 B1 subunits, respectively (13–15), have been associated with early-onset cases of distal renal tubular acidosis (dRTA), which suggests that the segmental distribution of IC-specific isoforms of V-ATPase could be acquired during early infancy.

In this study, we used real-time reverse transcription–PCR (RT-PCR) and *in situ* hybridization, coupled with immunoblotting and immunostaining analyses, to establish the comparative ontogeny of ubiquitous *versus* IC-specific subunits of V-ATPase during mouse nephrogenesis. In addition, on the basis of the structural model of V-ATPase (4), we assessed the relative mRNA expression of alternate isoforms in the adult mouse kidney. Finally, the subcellular distribution of V-ATPase subunits in the developing and mature kidney was compared with endosomal and lysosomal markers by analytical subcellular fractionation.

Materials and Methods

Mouse Kidney Samples

All samples were obtained from CD-1 mice (Iffa Credo, Brussels, Belgium), in accordance with National Institutes of Health guidelines for the care and use of laboratory animals and with the approval of the Committee for Animal Rights of the Université catholique de Louvain. Fetuses were removed and microdissected to isolate kidneys. Embryos from four different litters (average 12 embryos per litter) were collected daily from embryonic day 13.5 (E13.5) until day 5 after birth (newborn). Comparative studies were performed with eight 12-wk-old male kidneys.

Real-Time RT-PCR

Mouse kidney samples were homogenized in Trizol (Invitrogen, Merelbeke, Belgium) to extract total RNA. Total RNA samples (2.7 μg) were treated with DNase I (Invitrogen) and reverse-transcribed into cDNA using SuperScript II RNase H Reverse Transcriptase (Invitrogen). Specific primers for V-ATPase subunits, Foxi1, Pendrin (PDS), glyceraldehyde-3-phosphate dehydrogenase (GAPDH), cyclophilin, and hypoxanthine guanine phosphoribosyl transferase (HPRT1) were designed using Beacon Designer 2.0 (Premier Biosoft International, Palo Alto, CA) and are summarized in Table 1. Real-time PCR analyses were performed in duplicate with 200 nM of both sense and antisense primers in a final volume of 25 μl using 1 unit of Platinum TaqDNA Polymerase, 2 mM $MgSO_4$, 400 μM dNTP, and SYBR Green I (Molecular Probe, Leiden, The Netherlands) diluted to $1:10^5$. The PCR mixture contained 10 nM fluorescein for initial well-to-well fluorescence normalization. PCR conditions were settled as incubation at 94°C for 3 min followed by 40 cycles of 30 s at 95°C, 30 s at 61°C, and 1 min at 72°C. The melting temperature of PCR product was checked at the end of each PCR by recording SYBR green fluorescence increase upon slowly renaturating DNA. For each assay, standard curves were prepared by serial four-fold dilutions of mouse adult kidney cDNA. The efficiencies of the amplifications with each primer set were calculated from the slope of the standard curve [efficiency = $(10^{-1/\text{slope}}) - 1$] and were close to 100% (Table 1).

The relative mRNA expression of the various isoforms (A, a1, B2, E1, G1, C1, a4, B1, G3, and C2) was investigated in adult male kidneys (n = 8), after normalization to HPRT1, cyclophilin, and GAPDH [Ratio = $2^{\Delta Ct\,(\text{Reporter} - \text{Target Gene})}$]. The relative changes in mRNA levels of these alternate isoforms during ontogeny were determined by comparison with the adult mRNA level, after adjustment to GAPDH [Ratio = $(\text{Efficiency}_{\text{target gene}})^{\Delta Ct(\text{Adult} - \text{Sample})}/(\text{Efficiency}_{\text{GAPDH}})^{\Delta Ct\,(\text{Adult} - \text{Sample})}$]

Table 1. Primers used for real-time RT-PCR[a]

Primer Pair	Forward	Reverse	Length (bp)	Efficiency
V-ATPase				
Atp6v0a1	5′-GCTTGGGAAGGTCCAATTTC-3′	5′-GGCACCTCTGGGTTTTCACCG-3′	174	1.02 ± 0.01
Atp6v0a4	5′-CCCTGTATGGACATCAGCAA-3′	5′-GATTTCTGGTGCTTGGCTCT-3′	115	1.02 ± 0.04
Atp6v1e1	5′-GGCGCTCAGCGATGCAGATGT-3′	5′-CAAGGCGACCTTTCTCAATG-3′	134	1.05 ± 0.01
Atp6v1a1	5′-CGTCAGTATGATGGCCGACT-3′	5′-ACTCTGCCTGCTCGCTCATA-3′	147	0.99 ± 0.01
Atp6v1b1	5′-TGGACCAGGTCAAGTTTGC-3′	5′-CCCTGAAGTCCCTTCAAACA-3′	134	1.05 ± 0.02
Atp6v1b2	5′-TGAGCCGGAACTACCTATCCCA-3′	5′-GTGCCATCTGGTAATGTCAAGTGG-3′	136	1.01 ± 0.01
Atp6v1c1	5′-GGAAGTTTGCTAACGCGAAG-3′	5′-TACCATTTCTGCGAGCGTTT-3′	150	1.01 ± 0.01
Atp6v1c2	5′-GAAGGCCAACCTGGAGAACT-3′	5′-AAGCTTGACTTGGGGACGAT-3′	144	1.05 ± 0.03
Atp6v1g1	5′-TGAAGCAGGCCAAAGAAGAA-3′	5′-GTCATCTTCTCCCGGGTCT-3′	148	1.04 ± 0.02
Atp6v1g3	5′-CATGGTGTGCGACATGAAAC-3′	5′-CATCAGGTGCACAGTTGCAG-3′	140	1.03 ± 0.01
Foxi1	5′-CCTCTCCACCATGACAGCAT-3′	5′-TCCCATGGCTACTGAGGTTG-3′	155	1.06 ± 0.05
Pendrin	5′-TTTGGAGGTTTGCAGATTGG-3′	5′-TAATGGAGAGGATGCCGTTG-3′	154	1.07 ± 0.06
GAPDH	5′-TGCACCACCAACTGCTTAGC-3′	5′-GGATGCAGGGATGATGTTCT-3′	176	1.04 ± 0.03
Cyclophilin	5′-CGTCTCCTTCGAGCTGTTTG-3′	5′-CCACCCTGGCACATGAATC-3′	139	1.02 ± 0.02
HPRT1	5′-ACATTGTGGCCCTCTGTGTG-3′	5′-TTATGTCCCCCGTTGACTGA-3′	162	0.99 ± 0.01

[a]V-ATPase, vacuolar H+-ATPase; GAPDH, glyceraldehyde-3-phosphate dehydrogenase; HPRT1, hypoxanthine guanine phosphoribosyl transferase.

(16). Real-time RT-PCR results were confirmed by using another set of primers for each of V-ATPase subunits.

In parallel with the relative quantification described above, we cloned DNA plasmids for each subunit and GAPDH to determine copy numbers of V-ATPase subunits transcripts. The PCR products were cloned into a pTZ57R vector (Fermentas GmbH, Vilnius, Lithuania) and transformed in JM 107 Competent Cells (MBI Fermentas). LB-broth cultures (150 ml) of single colonies were grown up overnight skating at 200 rpm at 37°C. Plasmid purification was performed with the High Purity Plasmid Systems (Gentaur, Brussels, Belgium) according to the manufacturer's recommendations. Standard curves were generated from serial 10-fold dilutions of the purified plasmid that contained the appropriate cDNA, and regression analyses of the threshold cycle (Ct) values of standard dilution series were used to determine the amplification efficiency (data not shown). The absolute amount of mRNA molecules of V-ATPase subunits in mouse adult kidneys ($n = 8$) was determined by extrapolating the Ct values from the standard curves, according to the molecular weight of the plasmid (1.9×10^6 g/mol) and the Avogadro's number (1 mol = 6.022×10^{23} molecules), and then normalized to the GAPDH level in each sample. Each experiment was run in duplicate, with highly reproducible results.

In Situ *Hybridization*

Kidney samples were fixed in 4% formaldehyde (Boehringer Ingelheim, Heidelberg, Germany) in 0.1 M phosphate buffer (pH 7.4) before embedding in paraffin as described (17). Five-micrometer-thick sections were deparaffinized, rehydrated. and treated for 45 min at 37°C with 1 mg/ml proteinase-K (Sigma, St. Louis, MO) in 100 mM Tris-HCl (pH 8.0) and 50 mM EDTA. Sections then were acetylated for 10 min in 0.25% acetic anhydride and 0.1 M triethanolamine (pH 8.0) and prehybridized for 1 h at 52°C (Foxi1) or 56°C (B1) in the hybridization mixture that contained 40% (vol/vol) formamide, 50% (wt/vol) dextran sulfate, 2% (vol/vol) Denhardt's solution, and 2× SSC (1× SSC = 150 mM NaCl and 15 mM sodium citrate) in a humidified chamber. A mixture of two Foxi1- or B1-specific oligonucleotide probes (Foxi1 5′-AGGCTGGGTGACCTTCGAAGGCTGGATAAAGGGAACCGGG-3′, 5′-GAGTGGCTGTGAGCACAGCCTCTGGCACTGCTCGCTCCTCT-3′; B1 5′-AACATGGGTTCAAGCCATAAAGGAGAAGGCTGCAGCTGG-3′, 5′-TCCATTTCAGTTACATCTTTGGAGGCGGGGCTTCTATAAT-3′) or of two control oligonucleotides with the complementary sequence was prepared by fluorescein-dUTP labeling of the 3′ ends (Amersham Biosciences, Piscataway, NJ). The sections then were hybridized overnight at 52°C (Foxi1) or 56°C (B1) with the hybridization mixture supplemented with 1.5 ng/ml labeled probes and washed with decreasing concentrations of SSC (4×, 2×, and 1×). All washes were carried out at room temperature for 2 × 10 min. The detection of hybridized fluorescein-labeled probes was performed according to the immunostaining procedure, described below.

Antibodies

Immunoblotting and immunostaining analyses were performed with well-characterized antibodies, including mAb against the E1 subunit of the V-ATPase (a gift of Dr. S. Gluck, University of California, San Francisco, CA) (6); β-actin (Sigma); fluorescein (Dako, Glostrup, Denmark); α1 Na^+/K^+-ATPase (Upstate Biotechnology Inc., Waltham, MA); rabbit polyclonal antibodies against a4 subunit (13); B1, B2, G1, and G3 subunits (17); A subunit (Wako Chemicals GmbH, Neuss, Germany); C1 subunit (Santa Cruz Biotechnology, Santa Cruz, CA); Rab5a (Santa Cruz Biotechnology); aquaporin-2 (AQP2; Sigma); podocin (a gift from C. Antignac, Inserm U574, Necker Hospital, Paris, France) (18); sheep polyclonal antibodies against megalin (a gift from P.J. Verroust, Saint-Antoine Medical Faculty, Paris, France) (8); type II carbonic anhydrase (CAII; Serotec, Oxford, UK); goat polyclonal antibodies against cathepsin D (Santa Cruz Biotechnology); and chicken polyclonal antibodies against pendrin (a gift from P. Kopp, Northwestern University, Chicago, IL).

Analytical Subcellular Fractionation

Kidneys from approximately 40 fetuses at E16.5 and dissected cortex and medulla from five adult mice were minced in 0.25 M sucrose and 3 mM imidazole buffer (pH 7.4) that contained Complete protease inhibitors (Roche, Vilvoorde, Belgium) and homogenized in a Potter-Elvehjem tissue homogenizer (Thomas Scientific, Swedesboro, NJ). A low-speed "nuclear" fraction was pelletted at 700 × *g* for 10 min and extracted twice by resuspension sedimentation. Pooled postnuclear supernatants were sedimented further at 100,000 × *g* for 60 min in a 50Ti fixed-angle rotor (Beckman, Palo Alto, CA). The supernatant (S), which represents the cytosolic fraction, was collected for further char-

acterization. The high-speed pellet (MLP fraction of postnuclear particles) was resuspended in 1 ml of homogenization buffer, mixed with 7 ml of 16% (vol/vol) Percoll (average final density 1.048 g/ml), layered over a 250-μl Percoll cushion, and centrifuged at 60,000 $\times$ *g* for 30 min in a 50Ti rotor into a self-generating gradient, after which 10 fractions of approximately 750 μl each, excluding the packed cushion, were collected from the bottom. Each fraction was analyzed for density (refractometry), total protein content (Lowry assay), and amount of the indicated antigens (immunoblotting).

Immunoblotting

Membrane extraction and immunoblotting were performed as described previously (19). Briefly, kidney samples were homogenized in ice-cold buffer [300 mM sucrose and 25 mM N-2-hydroxyethylpiperazine-N′-2-ethanesulfonic acid made to pH 7.0 with 1 M tris(hydroxymethyl)aminomethane (Tris)] that contained Complete protease inhibitors (Roche). The homogenate was centrifuged at 1000 $\times$ *g* for 15 min at 4°C, and the resulting supernatant was centrifuged at 100,000 $\times$ *g* for 120 min at 4°C. The pellet was suspended in ice-cold homogenization buffer, before determination of protein concentration and storage at −80°C. After resolution by SDS-PAGE and blotting on nitrocellulose, the membranes were incubated overnight at 4°C with primary antibodies, washed, incubated for 1 h at room temperature with appropriate peroxidase-labeled antibodies (Dako), washed again, and visualized with enhanced chemiluminescence. Normalization for β-actin was obtained after stripping the blots and reprobing with the anti–β-actin antibody. Specificity of the immunoblot was determined by incubation with nonimmune rabbit or mouse IgG (Vector Laboratories, Burlingame, CA) or control ascites fluid (Sigma). Densitometry analysis was performed with a Canon CanoScan8000F using the NIH Image V1.60 software. All immunoblots were performed at least in duplicate.

Immunostaining

After blocking endogenous peroxidase for 30 min with 0.3% hydrogen peroxide, sections were incubated with 10% normal goat serum for 60 min, before incubation with the primary antibodies diluted in PBS that contained 2% BSA for 60 min. After washing in 50 mM Tris-HCl, sections were incubated successively with biotinylated secondary anti-IgG antibodies, avidin-biotin peroxidase, and diaminobenzidine or aminoethylcarbazole (Vector Laboratories). For immunofluorescence studies, secondary antibodies were detected with Texas red–conjugated and FITC-conjugated avidin (Vector Laboratories). Sections were viewed under a Leica DMR coupled to a Leica DC300 digital camera (Leica, Heerbrugg, Switzerland). The specificity of immunostaining was tested by incubation (*1*) in the absence of primary antiserum and (*2*) with nonimmune rabbit serum or control rabbit or mouse IgG (Vector Laboratories).

Results

Relative Expression of V-ATPase Subunits in Adult Mouse Kidney

The recently updated structure of the V-ATPase contains at least 13 different subunits that form two functional domains, V0 and V1 (Figure 1). Before considering the expression of isoforms during mouse nephrogenesis, we performed comparative real-time RT-PCR quantification, with different reporter genes, to establish the relative mRNA expression of ubiquitous and IC-specific subunits in adult mouse kidney (Figure 2). These data were essentially confirmed by absolute real-time RT-PCR using standard curves of cloned DNA plasmids for the V-ATPase subunits and GAPDH (data not shown). These studies revealed striking differences in terms of relative expression

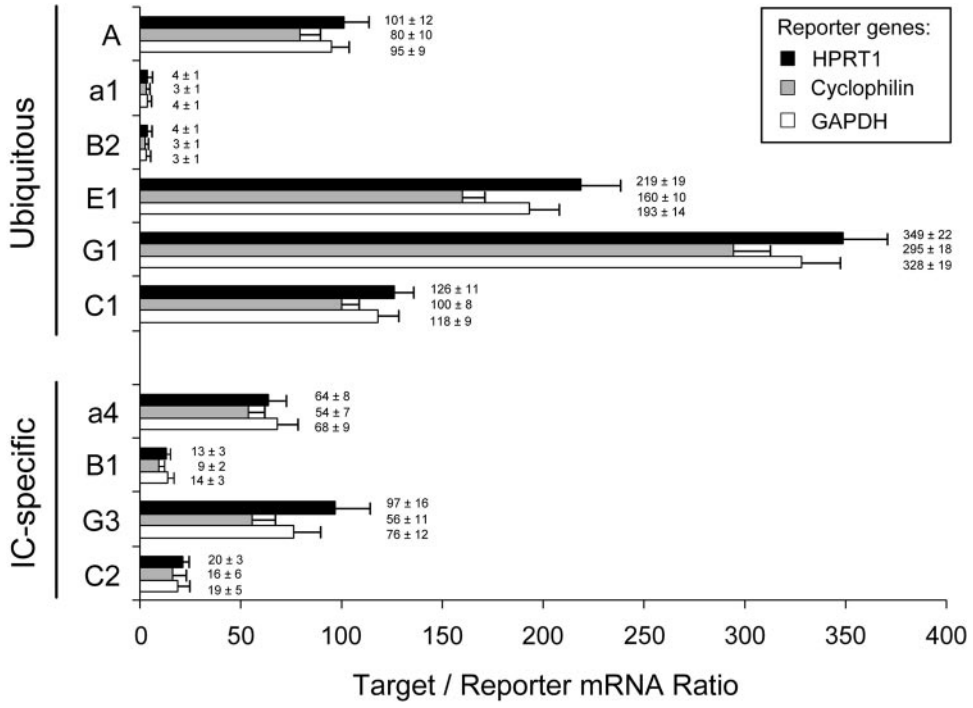

Figure 2. mRNA quantification of V-ATPase subunits. Real-time reverse transcription–PCR (RT-PCR) quantification of ubiquitous (A, a1, B2, E1, G1, and C1) and IC-specific (a4, B1, G3, and C2) subunits in mouse adult kidney (n = 8). The mRNA expression levels (mean ± SEM) were compared after adjustment to HPRT1 ($\times$50), cyclophilin ($\times 10^3$), or glyceraldehyde-3-phosphate dehydrogenase (GAPDH; $\times 2.10^3$) as reporter genes. HPRT1, hypoxanthine guanine phosphoribosyl transferase.

at the mRNA level that could not be explained by the structural stoichiometry of the V-ATPase complex shown in Figure 1. For instance, the A subunit was 20-fold more abundant than B2, although these subunits are considered to form the A3B3 catalytic core of the V1 domain. Moreover, comparative analysis of alternate isoforms inside ubiquitous (a1, B2, C1, and G1) or IC-specific (a4, B1, C2, and G3) pumps did not show a constant stoichiometry. These results suggest that the assembly of the V-ATPase complex results from important posttranscriptional modifications and/or reflects significant differences in the turnover of its various components.

Expression of V-ATPase Subunits mRNA in Developing Mouse Kidney

The differential expression patterns of ubiquitous and IC-specific V-ATPase subunits during mouse nephrogenesis were investigated using real-time RT-PCR analyses (Figure 3). The ubiquitous A, B2, E1, G1, and C1 subunits showed an early (E13.5) and stable expression (approximately 40% of the adult level) throughout nephrogenesis, reaching the adult level at birth (Figure 3A). Of note, the a1 isoform showed an earlier induction at E13.5 (approximately 135%) followed by a gradual decrease during late ontogeny and a second increase around birth. This particular developmental pattern is similar to that described for the endosomal kidney-specific chloride channel, ClC-5, and for the V0 d1 V-ATPase subunit (19,20). In contrast, the corresponding IC-specific B1, G3, C2, and a4 subunits were barely detected at E15.5 and showed a progressive induction during late ontogeny, like the anion transporter pendrin (Figure 3B). It must be noted that the forkhead transcription factor Foxi1, which is a member of the HFH/winged helix family, was detected from E15.5 (Figure 3B). These data show that the early expression of ubiquitous subunits of V-ATPase definitively contrasts with the later and more progressive appearance of Foxi1, pendrin, and IC-specific subunits.

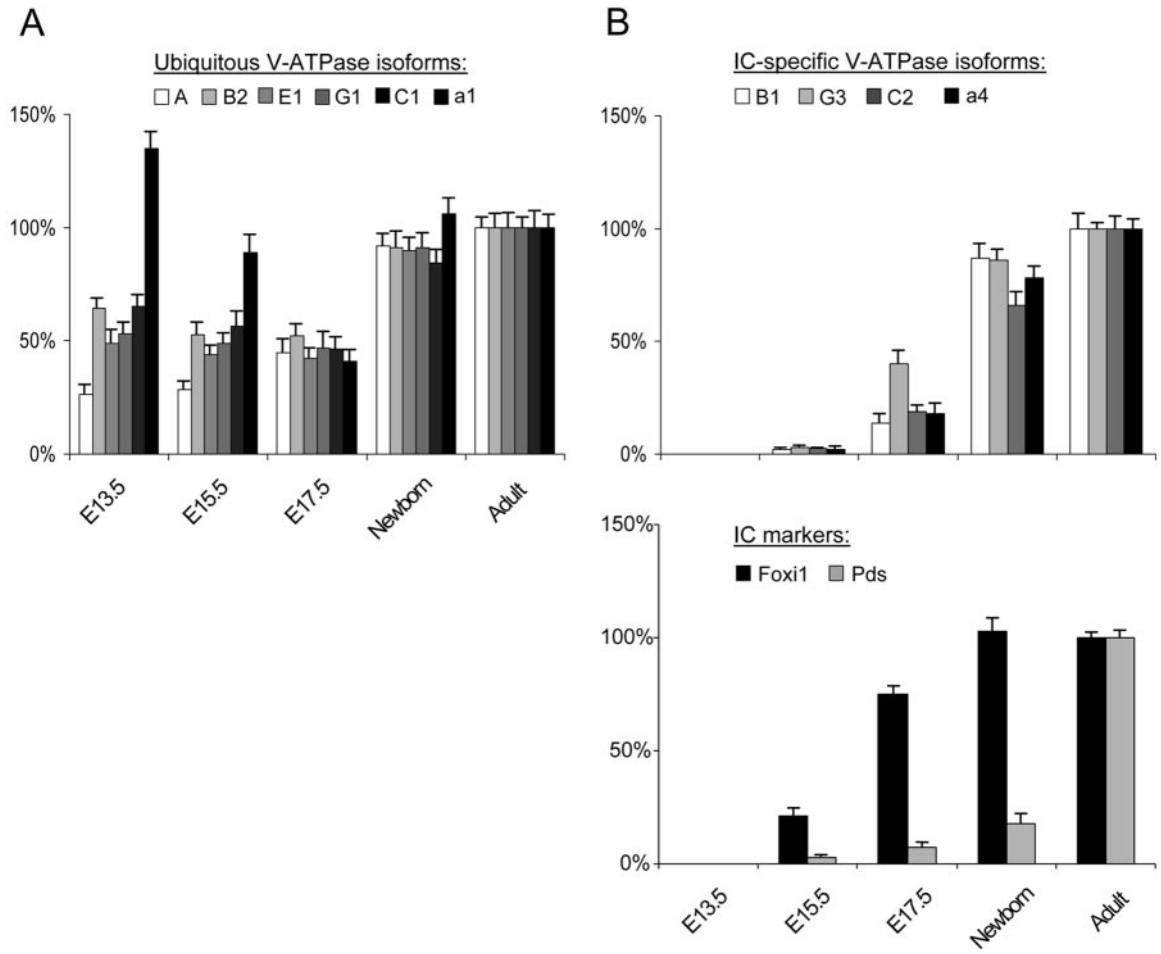

Figure 3. Expression of V-ATPase subunits in mouse developing kidney. Real-time RT-PCR quantification for mRNA expression of ubiquitous A, B2, E1, G1, C1, and a1 subunits (A) and IC-specific B1, G3, C2, and a4 isoforms, as well as Foxi1 and pendrin (pds) (B), during mouse nephrogenesis. The mRNA levels were first adjusted to GAPDH at every developmental stage, then normalized to the adult level set at 100% using the following formula: [Ratio = $(\text{Efficiency}_{\text{target}})^{\Delta Ct\,(\text{Adult} - \text{Sample})}$/ $(\text{Efficiency}_{\text{GAPDH}})^{\Delta Ct\,(\text{Adult} - \text{Sample})}$]. The early (embryonic day 13.5 [E13.5]) and stable expression of ubiquitous subunits during nephrogenesis clearly contrasts with the later and progressive appearance of IC-specific isoforms and pds, which follows the induction of the transcription factor Foxi1 at E15.5. Note that the a1 subunit is characterized by a bimodal developmental pattern.

Distribution of Forkhead Transcription Factor Foxi1 in Developing Mouse Kidney

The winged helix transcriptional activator Foxi1 has been located to the distal part of the nephron from E16.5 during mouse nephrogenesis (21) and recently implicated in IC differentiation along the CD (22). To investigate the putative link between Foxi1 and IC-specific V-ATPase isoforms expression, we performed *in situ* hybridizations on mouse developing kidney with fluorescein-labeled oligonucleotides directed against Foxi1 or B1 (Figure 4). At E15.5, Foxi1 was detected in some scattered cells of the medullary CD, whereas no signal was found in glomeruli, PT, and differentiating structures in the cortex (Figure 4A). At later stages, Foxi1 mRNA was identified in a subset of cells within distinct tubules in cortex and medulla (Figure 4C). In these cells, Foxi1 co-distributed with the IC-specific B1 V-ATPase subunit (Figure 4D). Altogether, the real-time RT-PCR and *in situ* hybridization data during mouse nephrogenesis strongly support the role of Foxi1 in the differentiation of IC along the CD.

Expression of V-ATPase Subunits in Developing Mouse Kidney

Well-characterized antibodies were used to evaluate the expression of ubiquitous and IC-specific V-ATPase subunits in mature and developing kidney (Figure 5). Postnuclear particles and high-speed supernatant, resolved by differential centrifugation of adult kidney samples, were analyzed by immunoblotting. In the adult kidney, approximately 20% of V1 subunits, *i.e.*, A, B2, E1 and G1, were detected in the cytosolic fraction, whereas the transmembrane a4, as well as the V1 C1 subunit, was associated only with membranes (Figure 5A). During nephrogenesis (Figure 5B), ubiquitous V-ATPase subunits (A, B2, E1, G1, and C1) were detected as early as E13.5 and gradually increased from E16.5 until birth. In contrast, the IC-specific subunit isoforms (a4, B1, and G3) and the anion exchanger pendrin were detected only from E16.5 and increased progressively during late nephrogenesis.

Segmental Distribution of V-ATPase Subunits in Developing Mouse Kidney

The segmental distribution of ubiquitous and IC-specific subunits in the developing mouse kidney was investigated using well-characterized antibodies against E1, B2, and a4 (Figure 6). No immunostaining for the IC-specific a4 subunit was detected at E14.5, by which time dispersed glomeruli and developing PT were observed in the inner cortex (Figure 6A). At E15.5, the immunoreactive signal was located in the apical area of scattered cells along the cortical (Figure 6B) and medullary CD (Figure 6C), whereas PT, ureteric buds, glomeruli, and differentiating structures remained unlabeled. By contrast, at this fetal stage, the distribution of ubiquitous E1 and B2 was acquired in PTC (Figure 6, D and I), as well as the distribution of E1 in IC (Figure 6D, inset). From E16.5, apical staining for a4 was detected in scattered IC (Figure 6, E, G, and H), clearly identified by co-distribution with CAII (Figure 6, F and G) but negative staining for AQP2 (Figure 6H). The distribution pattern of a4 in mouse developing kidney was restricted to IC (Figure 6J), similar to that observed in adult kidney (Figure 6K). The specificity of a4 staining was demonstrated with preimmune rabbit antibodies (Figure 6L). These results show that, in mouse developing kidney, the a4 subunit is detected progressively during IC differentiation, whereas the distribution of ubiquitous E1 and B2 includes both PTC and IC of the CD at an early stage.

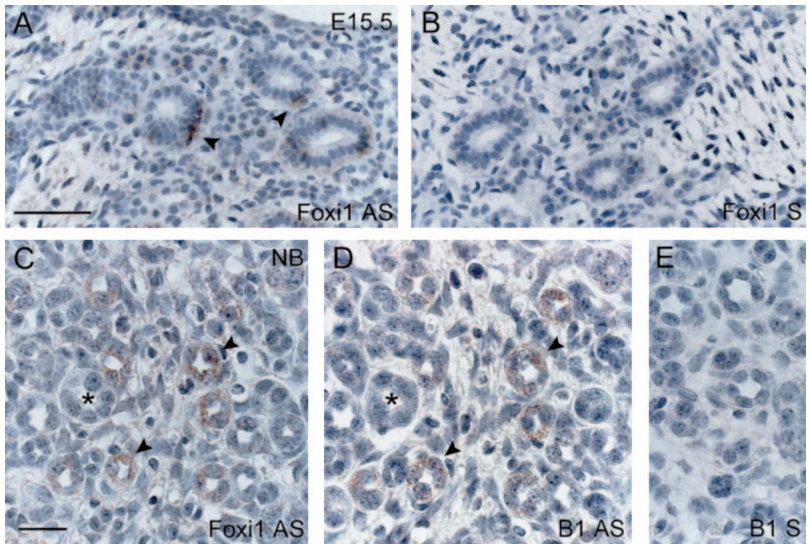

Figure 4. Distribution of Foxi1 and V-ATPase B1 subunit mRNA in mouse developing kidney. *In situ* hybridization for Foxi1 (A and C: antisense probe; B: sense); B1 V-ATPase subunit (D: antisense probe; E: sense) in the developing mouse E15.5 (A and B) and neonatal (C through E) kidney. At E15.5, Foxi1 mRNA is specifically detected in scattered cells within medullary collecting ducts (CD; A, arrowheads). In the newborn kidney, Foxi1 and B1 co-distribute in distinct cells within cortical CD (C and D, arrowheads on serial sections). No signal was detected when sense probes were used on consecutive sections (E). Bars = 50 μm in A and B; 20 μm in C through E.

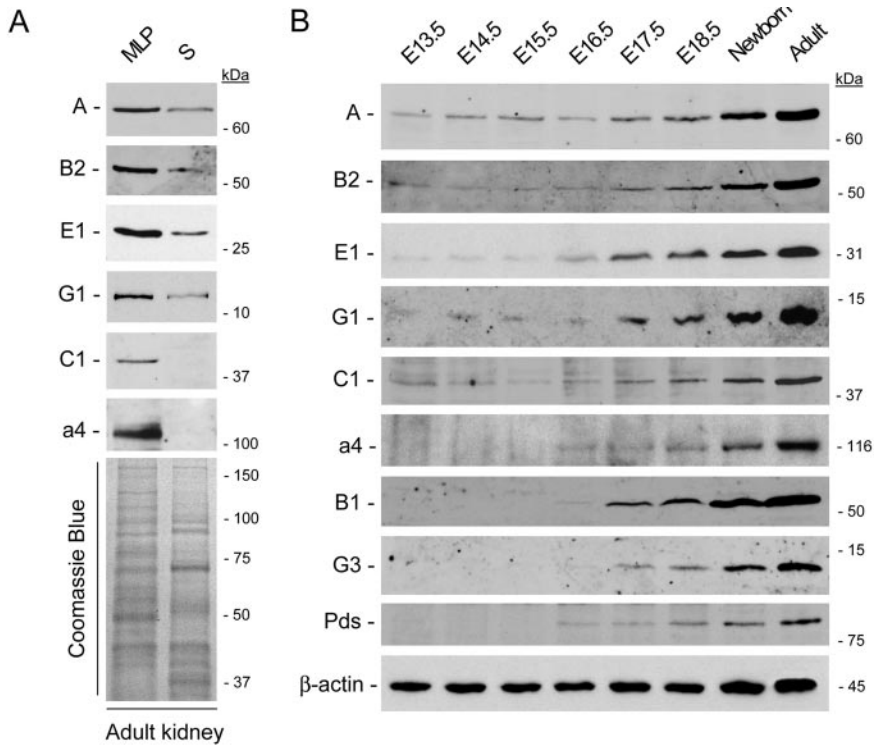

Figure 5. Expression of V-ATPase subunits in mouse developing kidney. (A) Relative expression of V1 A, B2, E1, G1, and C1, and V0 a4 in membrane (MLP) and cytosolic (S) compartments of adult mouse kidney. Equal loads (20 μg) of postnuclear particles (MLP 37% of total homogenate proteins) and high-speed supernatant (S 29% of total homogenate proteins) were analyzed. Densitometry analyses show that approximately 20% of V1 subunits are not associated with membranes at steady state. The transmembrane V0 a4 subunit, as well as the V1 C1, are not detected in the cytosolic fraction. (B) Representative immunoblots for ubiquitous A, B2, E1, G1, C1, and IC-specific a4, B1, and G3 V-ATPase subunits and pds in fetal (from E13.5 to E18.5), newborn, and adult mouse kidneys. A total of 20 μg of protein was loaded in each lane. Blots were probed with antibodies against A (1:1000), B2 (1:1000), E1 (1:100), G1 (1:500), C1 (1:1000), a4 (1:5000), B1 (1:1000), and G3 (1:500) subunits; pendrin (1:2000); and, after stripping, β-actin (1:10,000). Ubiquitous subunits are detected as early as E13.5 and gradually increase during late nephrogenesis, whereas the developmental pattern of IC-specific isoforms and pendrin is characterized by a later expression from E16.5.

Subcellular Fractionation in Percoll Gradients

In addition to its intracellular location where it mediates vesicle acidification, the V-ATPase is located at the cell surface of renal IC. We investigated the subcellular distribution of ubiquitous E1 and IC-specific a4 subunits in the mature and developing mouse kidney (Figure 7). Adult kidneys were dissected into cortex and medulla, and appropriate markers were analyzed by immunoblotting to validate the dissection (Figure 7A). Podocin and pendrin, as well as E1 and a4, were considerably enriched in the cortex, whereas AQP2 was detected mostly in the medulla (Figure 7B). These results confirm that the two parts of adult kidneys were purified adequately, as indicated by an enrichment ratio >30 (podocin *versus* AQP2). Next, the subcellular distribution of E1 and a4 in fetal kidney and adult cortex and medulla was compared (Figure 7C). Percoll gradients resolved a low-density peak (fractions 2 to 4) that comprised all (fetus) or the bulk (adult) of the early endosomal marker Rab5a from a high-density peak (fractions 9 and 10), including most of the lysosomal marker cathepsin D. In the three tissue samples, both V-ATPase subunits peaked in the low-density fractions, suggesting their major association with endosomes and not with lysosomes.

Discussion

In this study, we showed that ubiquitous and IC-specific isoforms of V-ATPase subunits are differentially expressed in mature kidney and during mouse nephrogenesis. The early expression of the ubiquitous A, B2, E1, G1, C1, and a1 subunits contrasts with the later and more progressive appearance of the IC-specific isoforms B1, G3, C2, and a4. The forkhead transcription factor Foxi1 mRNA was detected in IC from E15.5, with co-distribution with the B1 subunit in late nephrogenesis. The segmental distribution of E1 and B2 was acquired in PTC at E15.5, whereas a4 co-distributed with CAII in the IC during late nephrogenesis. Subcellular fractionation studies indicated a preferential location of both ubiquitous and IC-specific subunits to endosomes in both developing and mature kidneys.

The subunit composition of the bovine V-ATPase, previously determined by quantitative amino acid studies (1), was updated recently using electron microscopy and single-molecule image analysis (4). These investigations led to a structural model of the mammalian V-ATPase, which seems to be similar to the F_1F_0-ATP synthase in yeast (4). As a preliminary to the ontogeny analysis, real-time RT-PCR analyses in the adult kidney showed that the

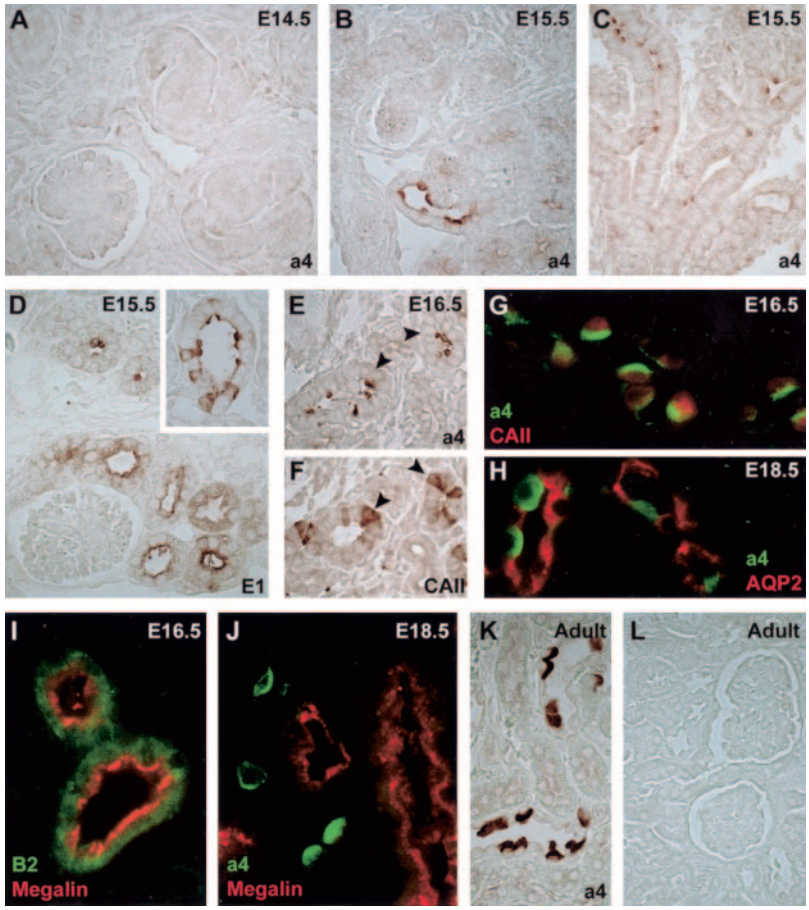

Figure 6. Segmental distribution of E1 and a4 V-ATPase subunits in mouse developing kidney. Immunostaining for a4 (all panels except D, F, I, and L), E1 (D), B2 (I), type II carbonic anhydrase (F and G), aquaporin 2 (AQP2; H), megalin (I and J), and negative control (L) in developing mouse kidney at E14.5 (A), E15.5 (B through D), E16.5 (E through G and I), and E18.5 (H and J) and in adult mouse kidney (K and L). No specific staining for a4 is observed at E14.5 (A). From E15.5, a4 is detected in the apical area of scattered cells of cortical (B) and medullary (C) CD, whereas proximal tubule cells (PTC) remain unstained. At this stage, the ubiquitous E1 and B2 are already expressed in developing PTC (D and I) and in IC of the medullary and cortical (D, inset) CD. At E16.5, apical staining for a4 is still present in scattered IC of the CD (E, arrowheads), clearly identified by co-staining positive for type II carbonic anhydrase (CAII; F, arrowheads, and G) but negative for AQP2 (H). This segmental distribution restricted to IC in mouse fetal kidney (J) is similar to that observed in the adult kidney (K). No staining for a4 subunit was observed with preimmune rabbit serum (L). Magnification, ×300 in A through F, K, and L; ×450 in G through J.

relative mRNA expression of V-ATPase subunits does not correspond to the expected stoichiometry. These results were confirmed by absolute mRNA quantification using standard curves from serial dilution of purified plasmids (data not shown). The ratio between the two methods varied between 0.8 and 1.8 according to the subunits, in agreement with previous comparative studies (23). This variability is attributed to distinct primer efficiency and, overall, cumulative errors introduced by the additional steps of the absolute mRNA quantification (spectrophotometry, calculations of molecular weight) (24). Thus, the relative method, using primer sets of similar efficiency (Table 1) and three distinct internal standards, was preferred to compare the abundance of V-ATPase subunit transcripts in one single kidney sample. The comparative mRNA quantification of subunits demonstrates a variable expression from ubiquitous to IC-specific V-ATPase complexes. Although minimal and/or limited correlation between the mRNA and protein levels is most often reported, the degree of correlation could vary according to subcellular localization or functional category (25). In the case of the renal V-ATPase complex, a first hypothesis could be significant variations in the turnover of the subunits that compose the complex, as well as a differential regulation of subunit mRNA stability (26). Because *in vivo* regulation of V-ATPase, which involves the reversible dissociation of V1 from V0 domain (27), does not require new protein synthesis but an efficient microtubular system (28), a second hypothesis could be posttranscriptional modifications during subunit synthesis and V-ATPase assembly. For instance, rearrangements during the formation of V0 and V1 domains might stabilize each of these subunits by tight interactions and/or mutual chaperoning. Of interest, a selective posttranscriptional control of protein expression levels among loci of the V-ATPase complex has been shown to operate in *Saccharomyces cerevisiae* (29).

The molecular events that occur in renal tubular cells after the onset of glomerular filtration, which starts at E14 in mouse

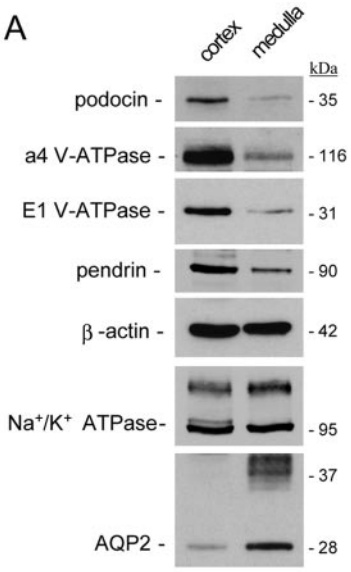

B

	cortex/medulla
podocin	6.8
a4 V- ATPase	5.3
E1 V- ATPase	3.7
pendrin	3.1
β-actin	1.2
Na+/K+ - ATPase	0.9
AQP2	0.2

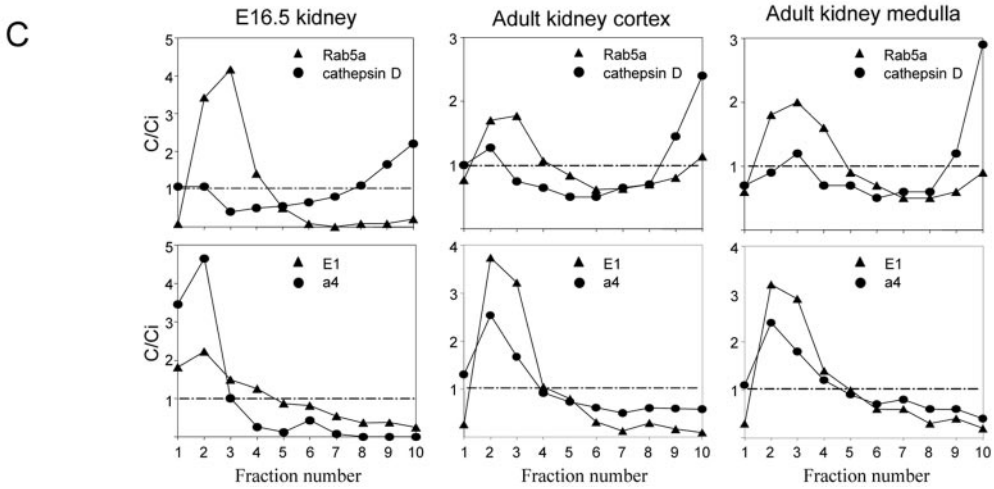

Figure 7. Localization and subcellular distribution of V-ATPase subunits in fetal and adult (cortex and medulla) mouse kidneys. (A) Representative immunoblots for podocin, IC-specific a4 and ubiquitous E1 V-ATPase subunits, pendrin, β-actin, Na^+/K^+-ATPase, and AQP2 in cortex and medulla of adult mouse kidney. Thirty micrograms of protein were loaded in each lane. Podocin (1:5000), a4 (1:5000), E1 (1:100), and pendrin (1:1000) are highly enriched in the dissected cortex and depleted in the dissected medulla; β-actin (1:10,000) and Na^+/K^+-ATPase (1:5000) are equally expressed in both tissues; AQP2 (1:2000) is detected mostly in the dissected medulla. (B) The relative enrichment of these markers, based on densitometry. (C) Percoll gradients of total fetal (E16.5) and adult (cortex and medulla) mouse kidneys. Distributions after centrifugation are presented in comparison with the initial concentration (C/Ci) so that values >1 reflect organelle enrichment and values <1 reflect organelle depletion. For immunoblotting analyses, equal volumes were loaded in each lane. The gradients resolve a low-density peak (fractions 2 to 4), including early endosomes (Rab5a), from a high-density peak (fractions 9 and 10), enriched in lysosomes (cathepsin D). The two V-ATPase subunits peak in the low-density fractions, which suggests their major association with endosomes and not with lysosomes in both developing and adult (cortex and medulla) kidneys.

(30), remain incompletely elucidated. Recent evidence suggests that different steps of kidney organogenesis are reflected by clusters of differentially regulated genes, including transporters and ions-motive ATPases, under the control of specific transcription activators (9,31). In rats (32) and humans (33), PT endocytic activity is effective during nephrogenesis or immediately after birth. Both the receptor-mediated endocytic pathway and the apical targeting within PTC (8) depend on a correct vacuolar acidification, which is mediated by V-ATPase in PTC. Our real-time RT-PCR and immunoblotting analyses show an early and stable expression of ubiquitous isoforms of V-ATPase subunits during nephrogenesis, which is in keeping with its essential role for early mouse development (12). It is interesting that the endosomal a1 subunit shows an early induction, a progressive decrease during late ontogeny, and a novel induction around birth. Such a biphasic developmental pattern is also described for the renal chloride channel ClC-5 that co-locates with V-ATPase in PT endosomes (34), as well as

for the V0 d1 subunit (20). ClC-5 is mutated in Dent's disease, an X-linked renal tubular disorder characterized by a major and early defect in the PT endocytic pathway (35). Thus, besides the stable expression of ubiquitous subunits, ClC-5 and a1 isoform, which are considered to target correctly V-ATPase complex to appropriate intracellular compartments (36), both are expressed simultaneously in PTC as early as the glomerular filtration starts. These essential components of the endocytotic process, responsible for the reabsorption of amino acids, vitamins, and minerals, may indeed be required early for correct growth and development. Analytical subcellular fractionation clearly resolved the two V-ATPase subunits from lysosomes, as assessed by the cathepsin D distribution, and rather pointed to a primary endosomal location, as shown by co-distribution with Rab5a. This low-density pattern is identical to what we recently reported for ClC-5 (8). Thus, kidney endosomes seem to be well equipped with electrogenic proton pumps and a chloride conductance, both in the adult and the fetus.

The IC constitute approximately one third of the cells that line the mouse CD (37). Although both α- and β-IC are characterized by high CAII activity, they differ by the selective polarity of V-ATPase and type 1 anion exchanger, allowing them to participate in proton (α type) or bicarbonate (β type) urinary secretion (7). The differentiation and maturation of the various cell types within the CD is poorly understood. Studies in the rat have shown that V-ATPase and CAII are detected simultaneously in IC at the end of gestation (38). During the first weeks of life, IC continue their maturation but are partially removed from specific parts of the CD by apoptosis or luminal extrusion (39). Recently, the winged helix transcriptional factor Foxi1, previously located in mouse fetal distal nephron (21), was shown to play an essential role in IC differentiation from epithelial precursor cells in the CD (22). In addition, Foxi1 is regarded as an upstream regulator of the anion transporter pendrin during inner ear development (40). Indeed, mice that lack Foxi1 showed a lack of differentiation of the distal nephron, leading to dRTA (22), as well as a sensorineural deafness resembling that of Pendred syndrome (40). Our description of the developmental expression of Foxi1, IC-specific V-ATPase isoforms, and pendrin provides additional information on CD maturation in mouse. Real-time RT-PCR showed that IC-specific subunits B1, G3, C2, and a4, as well as pendrin, are expressed later than the ubiquitous isoforms, with a progressive induction after Foxi1 appearance (E15.5). *In situ* hybridization showed that at E15.5, Foxi1 is expressed in scattered cells of the medullary CD. At later stages, Foxi1 is identified in distinct cells within tubules in the cortex and outer medulla, in which it co-distributes with the IC-specific B1 subunit. *In silico* studies (http://mordor.cgb.ki.se/cgi-bin/CONSITE/consite) indicate that gene promoters of IC-specific markers, such as type 1 anion exchanger, AE4, pendrin, or IC-specific V-ATPase subunits, exhibit Foxi1 DNA binding consensus sequence (21,22). Immunoblot studies showed a coordinate expression of the IC-specific subunits and pendrin at approximately E16.5, with immunolocalization of a4 and CAII in IC. Of note, subcellular fractionation showed that, in both fetal (E16.5) and adult kidneys, a4 and E1 subunits are located mostly in endosomes. This observation corroborates a dynamic process that occurs in IC, which involves regulated exocytic insertion of V-ATPase from a vesicular pool to the plasma membrane (41). Taken together, the mRNA and protein data support the case for a differential but coordinate regulation of IC-specific *versus* ubiquitous V-ATPase subunits during kidney development.

The comparative ontogeny of V-ATPase subunits helps us understand the pathophysiology of inherited renal disorders such as Dent's disease and dRTA. Dent's disease, which is due to inactivating mutations in *CLCN5* that presumably lead to impaired endosomal acidification in PTC, is characterized by low molecular weight proteinuria that can be detected within the first weeks of life (35). These clinical findings, which suggest that the molecular mechanisms that ensure endosomal acidification must be acquired at birth (19), have their counterpart in our demonstration of a parallel induction of the endosomal a1 isoform and ClC-5 that culminates at birth. Given the essential role of V-ATPase in early embryogenesis and its large tissue distribution, no mutation of any ubiquitous V-ATPase subunits has ever been reported, being definitively not compatible with life (12). In contrast, mutations in IC-specific isoforms have been associated with human dRTA (13–15). Some well-documented patients show clinical manifestations of dRTA during infancy, which suggests that the segmental expression of these IC-specific isoforms of V-ATPase must be acquired early, as indeed documented here.

In conclusion, our data demonstrate that ubiquitous and IC-specific isoforms of V-ATPase subunits are differentially expressed during mouse nephrogenesis. These results provide new insights into the segmental distribution of V-ATPase complexes in the kidney and represent a useful tool to investigate further any newly discovered subunit isoforms. The deciphering of the complex maturation of PTC and IC along the distal nephron also helps us understand the pathophysiology of renal tubular disorders.

Acknowledgments

These investigations were supported by the Université catholique de Louvain, the Fonds National de la Recherche Scientifique (FNRS), the Forton Foundation, Concerted Research Actions, Inter-University Attraction Poles, and the EuReGene integrated project of the European Community (FP6). F.J. is a research fellow of the FNRS, and C.P. is a research fellow of the FRIA.

We are grateful to Y. Cnops, M. Leruth, L. Wenderickx, and P. Henriet for excellent technical help and discussion and to M. Futai, P. Gailly, A. Goffinet, N. Tajeddine, and M.-F. van den Hove for material.

References

1. Nishi T, Forgac M: The vacuolar H+-ATPases: Nature's most versatile proton pumps. *Nat Rev Mol Cell Biol* 3: 94–103, 2002
2. Nelson N, Harvey WR: Vacuolar and plasma membrane proton-adenosinetriphosphatases. *Physiol Rev* 79: 361–385, 1999
3. Wagner CA, Finberg KE, Breton S, Marshansky V, Brown D, Geibel JP: Renal vacuolar H+-ATPase. *Physiol Rev* 84: 1263–1314, 2004
4. Wilkens S, Takao I, Forgac M: Three-dimensional structure of the vacuolar ATPase—Localization of subunit H by difference imaging and chemical cross-linking. *J Biol Chem* 279: 41942–41949, 2004

5. Borthwick KJ, Karet FE: Inherited disorders of the H+-ATPase. *Curr Opin Nephrol Hypertens* 11: 563–568, 2002
6. Brown D, Hirsch S, Gluck S: Localization of a proton-pumping ATPase in rat kidney. *J Clin Invest* 82: 2114–2126, 1988
7. Giebisch G, Windhager E: Transport of acids and bases. In: *Medical Physiology*, edited by Boron WF, Boulpaep EL, Philadelphia, Saunders, 2004, pp 845–860
8. Christensen EI, Devuyst O, Dom G, Nielsen R, Van der Smissen P, Verroust P, Leruth M, Guggino WB, Courtoy PJ: Loss of chloride channel, ClC-5, impairs endocytosis by defective trafficking of megalin and cubilin in kidney proximal tubules. *Proc Natl Acad Sci U S A* 100: 8472–8477, 2003
9. Schwab K, Patterson LT, Aronow BJ, Luckas R, Liang HC, Potter SS: A catalogue of gene expression in the developing kidney. *Kidney Int* 64: 1588–1604, 2003
10. Bonnici B, Wagner CA: Postnatal expression of transport proteins involved in acid-base transport in mouse kidney. *Pflugers Arch* 448: 16–28, 2004
11. Satlin LM, Woda CB, Schwartz GJ: Development of function in the metanephric kidney. In: *The Kidney, from Normal Development to Congenital Disease,* edited by Vize PD, Woolf AS, Bard JBL, Orlando, Academic Press (Elsevier), 2003, pp 267–326
12. Inoue H, Noumi T, Nagata M, Murakami H, Kanazawa H: Targeted disruption of the gene encoding the proteolipid subunit of mouse vacuolar H+-ATPase leads to early embryonic lethality. *Biochem Biophys Acta* 1413: 130–138, 1999
13. Smith AN, Skaug J, Choate KA, Nayir A, Bakkaloglu A, Ozen S, Hulton SA, Sanjad SA, Al-Sabban EA, Lifton RP, Scherer SW, Karet FE: Mutations in ATP6N1B, encoding a new kidney vacuolar proton pump 116-kDa subunit, cause recessive distal renal tubular acidosis with preserved hearing. *Nat Genet* 26: 71–75, 2000
14. Karet FE, Finberg KE, Nelson RD, Nayir A, Mocan H, Sanjad SA, Rodriguez-Soriano J, Santos F, Cremers CW, Di Pietro A, Hoffbrand BI, Winiarski J, Bakkaloglu A, Ozen S, Dusunsel R, Goodyer P, Hulton SA, Wu DK, Skvorak AB, Morton CC, Cunningham MJ, Jha V, Lifton RP: Mutations in the gene encoding B1 subunit of H+-ATPase cause renal tubular acidosis with sensorineural deafness. *Nat Genet* 21: 84–90, 1999
15. Stover EH, Borthwick KJ, Bavalia C, Eady N, Fritz DM, Rungroj N, Giersch AB, Morton CC, Axon PR, Akil I, Al-Sabban EA, Baguley DM, Bianca S, Bakkaloglu A, Bircan Z, Chauveau D, Clermont MJ, Guala A, Hulton SA, Kroes H, Li Volti G, Mir S, Mocan H, Nayir A, Ozen S, Rodriguez Soriano J, Sanjad SA, Tasic V, Taylor CM, Topaloglu R, Smith AN, Karet FE: Novel ATP6V1B1 and ATP6V0A4 mutations in autosomal recessive distal renal tubular acidosis with new evidence for hearing loss. *J Med Genet* 39: 796–803, 2002
16. Pfaffi MW: A new mathematical model for relative quantification in real-time RT-PCR. *Nucleic Acids Res* 29: 2004–2007, 2001
17. Sun-Wada GH, Murata Y, Namba M, Yamamoto A, Wada Y, Futai M: Mouse proton pump ATPase C subunit isoforms (C2-a and C2-b) specifically expressed in kidney and lung. *J Biol Chem* 278: 44843–44851, 2003
18. Roselli S, Gribouval O, Boute N, Sich M, Benessy F, Attie T, Gubler MC, Antignac C: Podocin localizes in the kidney to the slit diaphragm area. *Am J Pathol* 160: 131–139, 2002
19. Jouret F, Igarashi T, Gofflot F, Wilson PD, Karet FE, Thakker RV, Devuyst O: Comparative ontogeny, processing, and segmental distribution of the renal chloride channel, ClC-5. *Kidney Int* 65: 198–208, 2004
20. Smith AN, Jouret F, Bord S, Borthwick KJ, Al-Lamki RS, Wagner CA, Ireland DC, Cormier-Daire V, Frattini A, Villa A, Kornak U, Devuyst O, Karet FE: Vacuolar H+-ATPase d2 subunit: Molecular characterization, developmental regulation, and localization to specialized proton pumps in kidney and bone. *J Am Soc Nephrol* 16: 1245–1256, 2005
21. Overdier DG, Ye H, Peterson RS, Clevidence DE, Costa RH: The winged helix transcriptional activator, HFH-3, is expressed in the distal tubules of embryonic and adult mouse kidney. *J Biol Chem* 272: 13725–13730, 1997
22. Blomqvist SR, Vidarsson H, Fitzgerald S, Johansson BR, Ollerstam A, Brown R, Persson AE, Bergstrom GG, Enerback S: Distal renal tubular acidosis in mice that lack the forkhead transcription factor, Foxi1. *J Clin Invest* 113: 1560–1570, 2004
23. Rose'Meyer RB, Mellick AS, Garnham BG, Harrison GJ, Massa HM, Griffiths LR: The measurement of adenosine and estrogen receptor expression in rat brains following ovariectomy using quantitative PCR analysis. *Brain Res Brain Res Protoc* 11: 9–18, 2003
24. Freeman WM, Walker SJ, Vrana KE: Quantitative RT-PCR: Pitfalls and potential. *Biotechniques* 26: 112–122, 1999
25. Greenbaum D, Colangelo C, Williams K, Gerstein M: Comparing protein abundance and mRNA expression levels on a genomic scale. *Genome Biol* 4: 117, 2003
26. Wang SP, Krits I, Bai S, Lee BS: Regulation of enhanced vacuolar H+-ATPase expression in macrophages. *J Biol Chem* 277: 8827–8834, 2002
27. Kane PM: Disassembly and reassembly of the yeast vacuolar H+-ATPase in vivo. *J Biol Chem* 270: 17025–17032, 1995
28. Xu T, Forgac M: Microtubules are involved in glucose-dependent dissociation of the yeast vacuolar H+-ATPase in vivo. *J Biol Chem* 276: 24855–24861, 2001
29. Washburn MP, Koller A, Oshiro G, Ulaszek RR, Plouffe D, Deciu C, Winzeler E, Yates JR 3rd: Protein pathway and complex clustering of correlated mRNA and protein expression analyses in *Saccharomyces cerevisiae. Proc Natl Acad Sci U S A* 100: 3107–3112, 2003
30. Loughna S, Landels E, Woolf AS: Growth factor control of developing kidney endothelial cells. *Exp Nephrol* 4: 112–118, 1996
31. Stuart RO, Bush KT, Nigam SK: Changes in global gene expression patterns during development and maturation of the rat kidney. *Proc Natl Acad Sci U S A* 98: 5649–5654, 2001
32. Smaoui H, Schaeverbeke M, Mallie JP, Schaeverbeke J: Transplacental effects of gentamicin on endocytosis in rat renal proximal tubule cells. *Pediatr Nephrol* 8: 447–450, 1994
33. Mussap M, Fanos V, Piccoli A, Zaninotto M, Padovani EM, Plebani M: Low molecular mass proteins and urinary enzymes in amniotic fluid of healthy pregnant women at progressive stages of gestation. *Clin Biochem* 29: 51–56, 1996
34. Devuyst O, Christie PT, Courtoy PJ, Beauwens R, Thakker RV: Intra-renal and subcellular distribution of the human chloride channel, ClC-5, reveals a pathophysiological basis for Dent's disease. *Hum Mol Genet* 8: 247–257, 1999
35. Scheinman SJ: X-linked hypercalciuric nephrolithiasis: Clinical syndromes and chloride channel mutations. *Kidney Int* 53: 3–17, 1998
36. Manolson MF, Wu B, Proteau D, Taillon BE, Roberts BT, Hoyt MA, Jones EW: STV1 gene encodes functional homo-

logue of 95-kDa yeast vacuolar H+-ATPase subunit Vph1p. *J Biol Chem* 269: 14064–14074, 1994
37. Teng-umnuay P, Verlander JW, Yuan W, Tisher CC, Madsen KM: Identification of distinct subpopulations of intercalated cells in the mouse collecting duct. *J Am Soc Nephrol* 7: 260–274, 1996
38. Kim J, Tisher CC, Madsen KM: Differentiation of intercalated cells in developing rat kidney: An immunohistochemical study. *Am J Physiol* 266: F977–F990, 1994
39. Kim J, Cha JH, Tisher CC, Madsen KM: Role of apoptotic and nonapoptotic cell death in removal of intercalated cells from developing rat kidney. *Am J Physiol* 270: F575–F592, 1996
40. Hulander M, Kiernan AE, Blomqvist SR, Carlsson P, Samuelsson EJ, Johansson BR, Steel KP, Enerback S: Lack of pendrin expression leads to deafness and expansion of the endolymphatic compartment in inner ears of Foxi1 null mutant mice. *Development* 130: 2013–2025, 2003
41. Brown D, Breton S: H+-ATPase-dependent luminal acidification in the kidney collecting duct and the epididymis/vas deferens: Vesicle recycling and transcytotic pathways. *J Exp Biol* 203: 137–145, 2000
42. Smith AN, Borthwick KJ, Karet FE: Molecular cloning and characterization of novel tissue-specific isoforms of the human vacuolar H(+)-ATPase C, G and d subunits, and their evaluation in autosomal recessive distal renal tubular acidosis. *Gene* 297: 169–177, 2002